accordance with institutional guidelines. This study was approved by the Institutional Review Committees of Chiba University (approval numbers 21-65 and 21-150). Human cord blood (hCB) $CD34^+$ cells with a purity of over 95% were purchased from Lonza (Basel, Switzerland). Frozen stock of the $CD34^+$ cells were thawed and plated at 5×10^5 cells/well in a six-well plate pre-coated with 25 μg/ml fibronectin fragment CH-296 (Takara Shuzo, Otsu, Shiga, Japan) and cultured in serum-free medium, StemSpan SFEM (Stem Cell Technologies, Vancouver, BC, Canada) in the presence of 100 ng/ml human stem cell factor (SCF) (PeproTech, Rocky Hill, NJ, USA) and 50 ng/ml human thrombopoietin (TPO) (PeproTech) for 16 h. Subsequently, 5×10^4 $CD34^+$ cells were injected intravenously into 8-week-old NOG mice which had been irradiated with 2.0 Gy X-ray 2 h before. It has been reported that human HSC are mostly cycling at the early time points post-transplantation in NOG mice, but enter the quiescent state by 18 weeks post-transplantation (Yahata et al. 2011). We assumed that 12 weeks post-transplantation human HSC are well repopulated and substantially quiescent in humanized mice. Therefore, we irradiated mice with the test doses as indicated at the 12th week after transplantation. The same situation was assumed after irradiation. Therefore, we sacrificed mice for analysis at the 12th week after irradiation.

Irradiation

Mice were irradiated on a rotating platform of the Hitachi MBR1520R X-ray machine (150 kV; 20 mA; dose-rate: 1.5 Gy/min; 0.5 mm aluminum and 0.1 mm copper filters). Irradiation doses were verified by performing dosimetry using nanoDot dosimeters (Landauer, Glenwood, IL, USA). For 4 weeks after irradiation, mice were fed with drinking water containing 0.17 mg/ml enrofloxacin.

Flow cytometry

Human cells in the BM and PB of recipient mice were stained with PE-Cy7-conjugated anti-human CD45, APC-conjugated anti-human CD34, PE-conjugated anti-human CD38, and APC-Cy7-conjugated anti-human CD3, PE-conjugated anti-human CD11b, or PE-Cy7-conjugated anti-human CD19 (BD Biosciences, San Jose, CA, USA). They were then analyzed and sorted on a FACS Aria II (BD Biosciences).

Quantitative real-time PCR analysis

Total RNA was isolated using TRIZOL LS solution (Invitrogen, Carlsbad, CA, USA) and reverse transcribed by the ThermoScript RT-PCR system (Invitrogen) with an oligo dT primer. Real-time quantitative PCR was performed with an ABI prism 7300 Thermal Cycler (Applied Biosystems, Foster City, CA, USA) using FastStart Universal Probe Master (Roche Diagnostics, Branchburg, NJ, USA). *GAPDH* expression was used to calculate relative expression levels. Probe numbers and primer sequences were: Probe #65, 5′-AGGTGGGTAGAGGGTCTGC-3′ and 5′-TCCAATTCCCCTGCAAACT-3′ for $p16^{INK4A}$; and probe #25, 5′-ctgacttcaacagcgacacc-3′ and 5′-tagccaaattcgttgtcatacc-3′ for *GAPDH*.

Immunostaining of γH2AX

Cells were incubated in a culture medium drop on slide glasses pre-treated with poly-L-lysine (Sigma, St Louis, MO, USA) for 2 h at 37°C. After fixation with 2% paraformaldehyde, treatment with 0.25% triton X-100, and blocking in 4% sheep serum for 30 min at room temperature, cells were incubated with purified anti-phospho-histone H2AX (Ser139) rabbit polyclonal antibody (Cell Signaling Technology, Danvers, MA, USA) for 12 h at 4°C. The cells were then washed and incubated with Alexa Flour 555-conjugated anti-rabbit IgG goat polyclonal antibody (Invitrogen) for 60 min at room temperature with protection from light. DNA was counterstained with 4′,6-diamidino-2-phenylindole (DAPI). Images were taken with a Keyence BZ-9000 fluorescence microscope.

Statistical analysis

The significance tests were performed by nonparametric methods: Jonckheere-Terpstra test for linear trend of percentage changes of human cells in the PB or BM across irradiation doses, and Chi-square test for the association between levels of γH2AX foci and irradiation dose in a 4×3 contingency table. Kaplan-Meier model was used for the difference of survival rates among mice irradiated with different doses. Statistical analysis was performed using SPSS (version 14.0, SPSS, Chicago, IL, USA).

Results

To evaluate the radiation effects on human HSPC in vivo, we transplanted 5×10^4 cord blood $CD34^+$ HSPC into NOG mice irradiated with 2.0 Gy via tail veins (Figure 1A). NOG is a mouse strain that exhibits severe immunodeficiency with lack of T, B, and natural killer (NK) cells. It has been reported that the human hematopoietic system can be effectively reconstructed in NOG mice by transplanting human HSC (Ito et al. 2002). At the 12th week after transplantation, the NOG mice showed considerably high chimerism, i.e., the median percentage of human $CD45^+$ hematopoietic cells in PB, was 61.5% (range, 37.6–74.4%, $n = 45$). The mice were randomly grouped into five categories and irradiated with 0, 0.5, 1.0, 2.0, or 4.0 Gy for each group (Figure 1A). NOG mice are susceptible to irradiation because of the *scid/scid* background (Fulop and Phillips 1990). Although the 50% lethal dose (LD_{50}) of NOG mice at a single exposure is 3.5 Gy (Ito M, personal communication), the LD_{50} of NOG mice already given prior exposure to 2.0 Gy of X-ray should be lower than 3.5 Gy. As expected, a majority of the mice irradiated with 2.0 Gy or more died within 12 weeks after irradiation (Figure 1B). Therefore, we focused on the mice that were exposed to 0.5 or 1.0 Gy of irradiation in this study.

The chimerism of human hematopoietic cells in PB of the control (non-irradiated) mice was about 50% after an additional 12 weeks (24 weeks in total after transplantation), and during the same period after irradiation the chimerism decreased in a dose-dependent manner while that of mouse hematopoietic cells increased (Figure 2A). Percentage of human $CD3^+$ T cells in PB increased at the expense of $CD19^+$ B cells and $CD11b^+$ myeloid cells during the latter 12 weeks

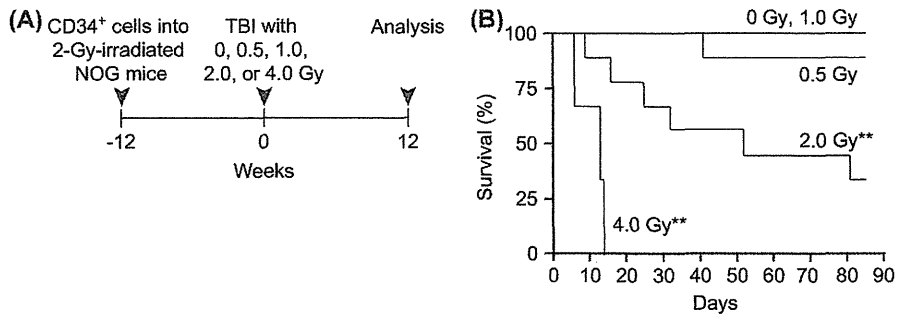

Figure 1. Experimental design and survival of humanized NOG mice after irradiation (A) Schema of experimental strategy. Cord blood $CD34^+$ HSPC (5×10^4) were transplanted into 8-week-old NOG mice irradiated with 2.0 Gy via tail veins. At the 12th week after transplantation, the mice were irradiated with 0, 0.5, 1.0, 2.0, or 4.0 Gy. After an additional 12 weeks (24 weeks in total after transplantation), the mice were sacrificed and subjected to detailed analysis. (B) A Kaplan-Meier survival curve of NOG mice after irradiation at doses indicated (0, 0.5, 1.0, 2.0, and 4.0 Gy; $n = 9$ in each dose group). 5×10^4 $CD34^+$ cells were injected intravenously into 8-week-old NOG mice irradiated with 2.0 Gy of X-rays. At the 12th week after transplantation, the chimerism of human $CD45^+$ hematopoietic cells in PB mononuclear cells (mouse $CD45^+$ cells plus human $CD45^+$ cells) was analyzed. Then, the mice were randomly grouped into five test radiation dose categories (0, 0.5, 1.0, 2.0, and 4.0 Gy). $^{**}P < 0.01$.

and irradiation enhanced these changes although they were not statistically significant (Figure 2B). Likewise, X-irradiation reduced the chimerism of human $CD45^+$ hematopoietic cells in BM as well as their absolute numbers in a dose-dependent manner (Figure 3A and B). Instead those of mouse hematopoietic cells in BM increased (Figure 3C). Percentages of human $CD34^+$ HSPC and human $CD34^+CD38^-$ HSC in $CD45^+$ human hematopoietic cells as well as their absolute numbers similarly declined (Figure 3B).

DNA damage is intimately linked to stem cell aging. Heritable DNA damage accrued in stem cells leads to stem cell senescence or apoptosis, which over time can lead to the shrinkage of the stem-cell pool and reduced regenerative capacity of stem cells (Rossi et al. 2008, Yahata et al. 2011). To evaluate the status of genomic damage in irradiated HSC, we next purified $CD34^+CD38^-$ HSC from the humanized mice at the 12th week after irradiation and determined the phosphorylation status of H2AX at Ser139, γH2AX, a marker of DNA breaks (Srivastava et al. 2009). Even the freshly isolated $CD34^+CD38^-$ cell fraction from human CB occasionally had γH2AX foci, and a similar cell fraction purified from non-irradiated humanized mice at 24 weeks post-transplantation also possessed such loci but included more cells with multiple γH2AX foci. Of note, compared to human HSC isolated from non-irradiated mice, those from irradiated mice showed significantly increased numbers of γH2AX foci (Figure 4A). We further examined the expression of $p16^{INK4A}$, a hallmark of aging of HSC (Janzen et al. 2006). Because of the limited number of $CD34^+CD38^-$ HSC

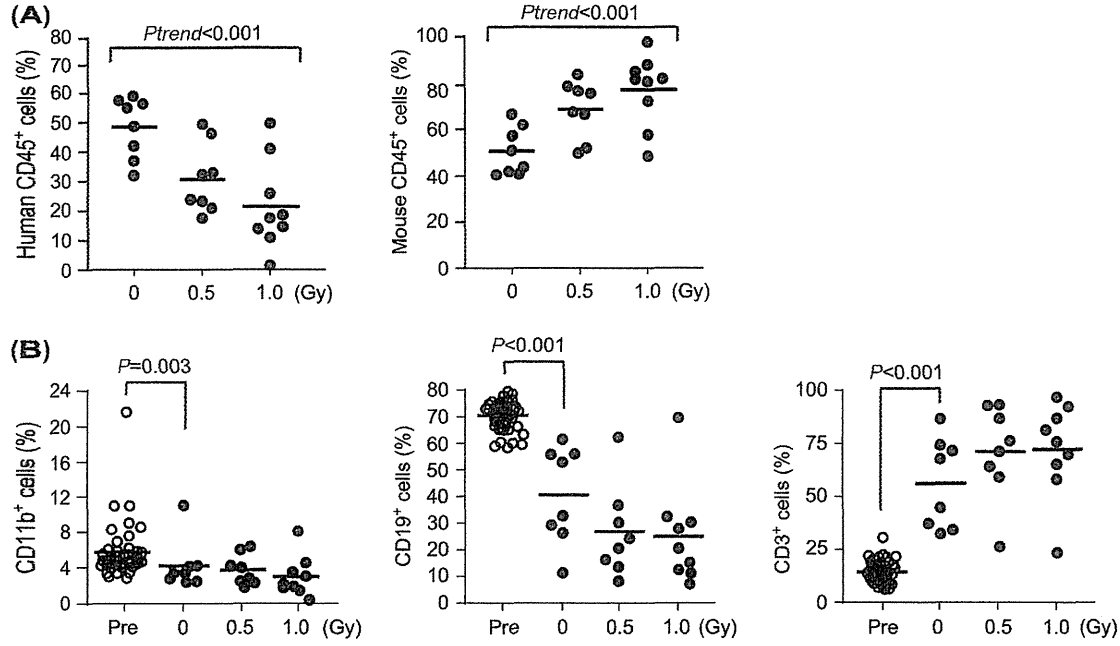

Figure 2. Contribution of human hematopoietic cells in PB of humanized mice following total-body irradiation (A) Changes in chimerism of human hematopoietic cells in PB after irradiation. At the 12th week after irradiation, the chimerism of $CD45^+$ human (left panel) and mouse (right panel) hematopoietic cells in PB of survived mice was analyzed, being indicated by dots ($n = 8$ or 9 in each dose group). Median values are indicated by bars. (B) The percentages of $CD11b^+$ myeloid cells, $CD19^+$ B cells, and $CD3^+$ T cells in $CD45^+$ human hematopoietic cells in PB of NOG mice just before the irradiation (Pre) and at 12 weeks after irradiation.

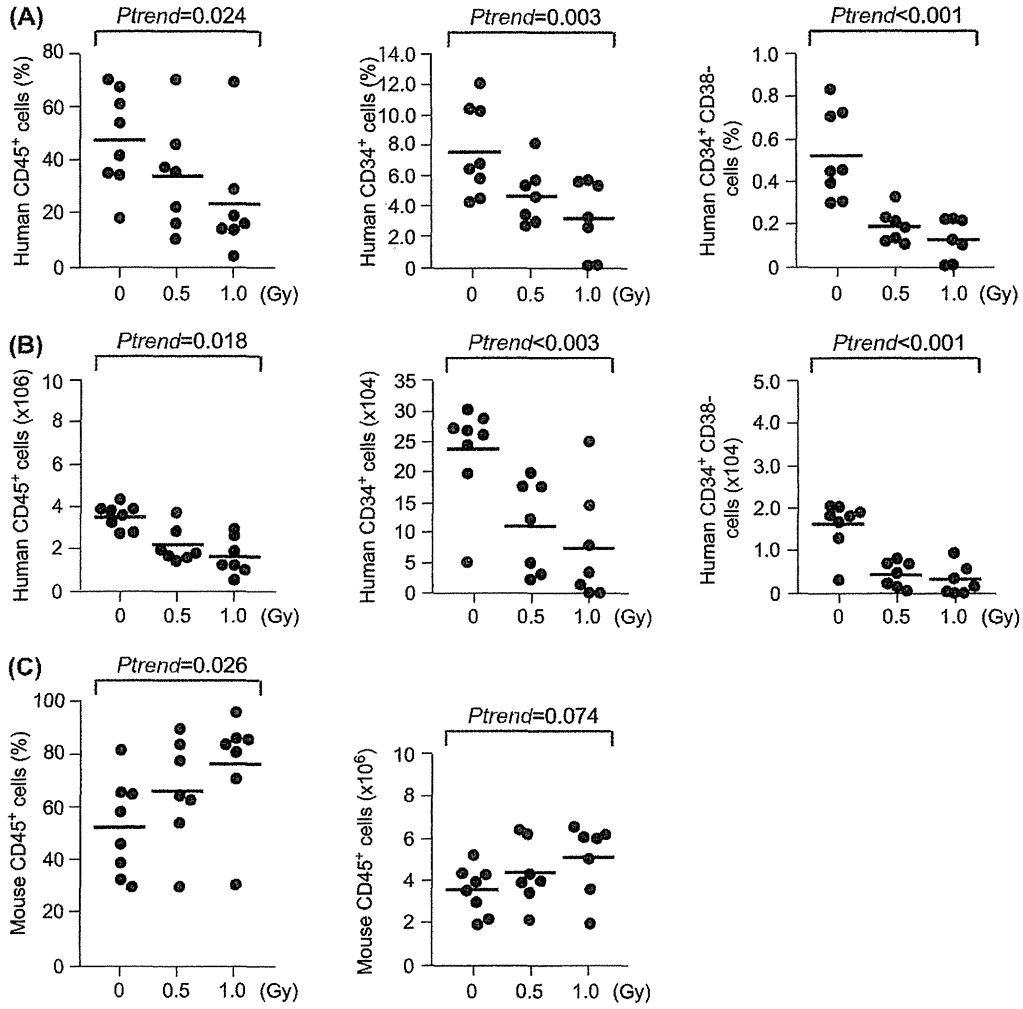

Figure 3. Contribution of human hematopoietic cells in BM of humanized mice following total-body irradiation (A) The chimerism of $CD45^+$ human hematopoietic cells in BM mononuclear cells and percentages of $CD34^+$ HSPC and $CD34^+CD38^-$ HSC in $CD45^+$ human hematopoietic BM cells in NOG mice at the 12th week after irradiation. (B) The absolute numbers of $CD45^+$ human hematopoietic cells, $CD34^+$ HSPC and $CD34^+CD38^-$ HSC in BM (bilateral femurs and tibiae) of NOG mice at the 12th week after irradiation. (C) The chimerism of $CD45^+$ mouse hematopoietic cells in BM mononuclear cells and the absolute numbers of $CD45^+$ mouse hematopoietic cells in BM (bilateral femurs and tibiae) of NOG mice at the 12th week after irradiation.

in the humanized NOG mice, we used $CD34^+$ HSPC which existed at the frequency 20-fold more than HSC for detection of $p16^{INK4A}$. Of note, expression of $p16^{INK4A}$ was detected only in HSPC from irradiated mice (Figure 4B).

Discussion

In this study, we demonstrated that the contribution of human cells to hematopoiesis in NOG mice declined in an X-ray dose-dependent manner at the 12th week after irradiation. This was in sharp contrast to an expectation that, following radiation exposure, highly-radiosensitive NOG mouse cells would be more seriously damaged than normal human cells. Decremented human hematopoiesis found in irradiated humanized mice was possibly caused by radiation dose-dependent decreases in the ability of transplanted and irradiated human HSC to repopulate following radiation injury. Indeed, increases in DNA damage and $p16^{INK4A}$ expression were observed in human HSPC of irradiated humanized mice, potentially leading to a diminished proliferation ability of human HSPC in the irradiated hosts. Although higher levels of DNA damage were supposed to induce higher levels of $p16^{INK4A}$, the level of $p16^{INK4A}$ in human HSPC from humanized mice irradiated with 0.5 Gy appeared to be higher than that from mice with 1.0 Gy. Because excessive $p16^{INK4A}$ causes cellular senescence or apoptosis, more HSPC might be depleted in mice that received a higher dose of X-ray. However, this study could not address this issue, due to a small sample size lacking statistical power for association analysis. Further investigations with a robust study design will be necessary to fully evaluate associations of $p16^{INK4A}$ levels with DNA damage, radiation dose and hematopoietic ability of human HSC.

It is known that HSC suffer from various stresses, including replicative and oxidative stresses, during serial transplantation and eventually lose self-renewal capacity (Ito et al.

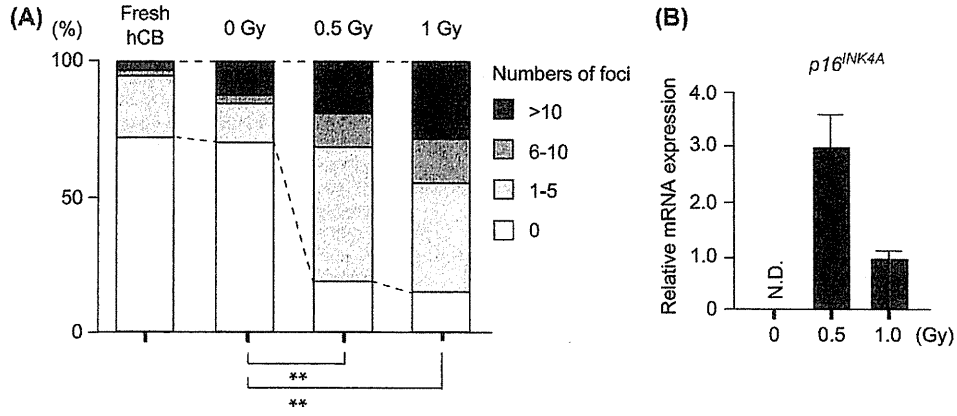

Figure 4. DNA damage and *p16*^{INK4A} expression in human HSC of irradiated humanized mice (A) DNA damage response of CD34$^+$CD38$^-$ HSC at the 12th week after irradiation. BM cells from the humanized mice irradiated with doses indicated (0, 0.5, and 1.0 Gy) were pooled for each dose group. CD34$^+$CD38$^-$ human HSC were then purified by cell sorting from the pooled BM cells and stained with anti-γH2AX. CD34$^+$CD38$^-$ HSC freshly isolated from hCB cells (Fresh hCB) were used as controls. Percentages of CD34$^+$CD38$^-$ HSC with indicated numbers of γH2AX foci are depicted. Counting of 40 cells was repeated three times in each dose group. $^{**}P < 0.001$ ($\chi^2 = 110.38$, df = 6). (B) Quantitative RT-PCR analysis of *p16*^{INK4A} in CD34$^+$ human HSPC from irradiated humanized mice. CD34$^+$ HSPC were purified by cell sorting as in (A). Relative expression levels of *p16*^{INK4A} mRNA were adjusted in reference to *GAPDH* mRNA expression levels and determined as a ratio to the expression level in the cells from NOG mice irradiated with 1.0 Gy. Data are shown as the mean ± SD for triplicate measurements. N.D. indicates not detected.

2006, Yahata et al. 2011). Serial transplantation of human HSC into immunodeficient mice triggers replicative stress that induces elevation of intracellular reactive oxygen species (ROS) levels along with the accumulation of persistent DNA damage within human HSC (Yahata et al. 2011). Thus, in our humanized mouse model, replicative and oxidative stresses caused by transplantation are likely to be augmented by radiation-induced DNA damage in transplanted human HSC. Restoration of HSC following marrow ablation is thought to highly rely on exogenous signals from the stem cell 'niche.' It has been reported that human and mouse HSC behave differently upon DNA damage following low-dose irradiation, i.e., DNA-damaged human HSC are prone to apoptosis and cannot well survive (Milyavsky et al. 2010) while similarly damaged mouse HSC tend to stay alive with competent DNA repair processes (Mohrin et al. 2010). However, there are considerable problems in terms of cross-reactivity of mouse molecules to human HSC, including cytokines, growth factors, and adhesion molecules. Furthermore, the NOG mice lack various immune cells, including T, B, and NK cells, that would normally be involved in producing supportive factors for HSC (Ito et al. 2002). In irradiated humanized mice, the mouse BM niche might provide less efficient survival signals for damaged human cells than for damaged mouse cells, and human hematopoiesis might become more compromised than mouse hematopoiesis. It is important to evaluate the consequence of DNA damage following irradiation in both human and mouse HSC in the same condition of BM niches. To this end, it would be challenging but may help to transplant human niche cells such as mesenchymal stem cells and/or stromal cells along with human HSC, or to use immunodeficient mice genetically engineered to express human cytokines such as stem cell factor and thrombopoietin (Rongvaux et al. 2011, Takagi et al. 2012).

The humanized mouse model in this study allowed us to assess the long-term radiation effects, including DNA damage, at doses of 0.5 and 1.0 Gy on human HSC residing in the BM microenvironment. We propose that humanized mice should be able to serve as a valuable tool for risk assessment after radiation exposure and also for evaluating efficacy of preventive and therapeutic agents.

Acknowledgements

We thank Makiko Yui for technical assistance.

Declaration of interest

The authors report no conflicts of interest. The authors alone are responsible for the content and writing of the paper.

This work was supported in part by the U.S. National Institute of Allergy and Infectious Diseases (NIAID Contract HHSN272200900059C). The views of the authors do not necessarily reflect those of the two governments.

The Radiation Effects Research Foundation (RERF), Hiroshima and Nagasaki, Japan, is a private, nonprofit foundation funded by the Japanese Ministry of Health, Labor, and Welfare and the U.S. Department of Energy, the latter in part through DOE Award DE-HS0000031 to the National Academy of Sciences.

References

Fulop GM, Phillips RA. 1990. The scid mutation in mice causes a general defect in DNA repair. Nature 347:479–482.

Hamasaki K, Imai K, Hayashi T, Nakachi K, Kusunoki Y. 2007. Radiation sensitivity and genomic instability in the hematopoietic system: Frequencies of micronucleated reticulocytes in whole-body X-irradiated BALB/c and C57BL/6 mice. Cancer Science 98: 1840–1844.

Ito K, Hirao A, Arai F, Takubo K, Matsuoka S, Miyamoto K, Ohmura M, Naka K, Hosokawa K, Ikeda Y, Suda T. 2006. Reactive oxygen species act through p38 MAPK to limit the lifespan of hematopoietic stem cells. Nature Medicine 12:446–451.

Ito M, Hiramatsu H, Kobayashi K, Suzue K, Kawahata M, Hioki K, Ueyama Y, Koyanagi Y, Sugamura K, Tsuji K, Heike T, Nakahata T. 2002. NOD/SCID/gamma (c) (null) mouse: An excellent recipient mouse model for engraftment of human cells. Blood 100:3175–3182.

Janzen V, Forkert R, Fleming HE, Saito Y, Waring MT, Dombkowski DM, Cheng T, DePinho RA, Sharpless NE, Scadden DT. 2006. Stem-cell ageing modified by the cyclin-dependent kinase inhibitor p16INK4a. Nature 443:421–426.

Kyoizumi S, McCune J M, Namikawa R. 1994. Direct evaluation of radiation damage in human hematopoietic progenitor cells in vivo. Radiation Research 137:76–83.

Milyavsky M, Gan OI, Trottier M, Komosa M, Tabach O, Notta F, Lechman E, Hermans KG, Eppert K, Konovalova Z, Ornatsky O, Domany E, Meyn MS, Dick JE. 2010. A distinctive DNA damage response in human hematopoietic stem cells reveals an apoptosis-independent role for p53 in self-renewal. Cell Stem Cell 7:186–197.

Mohrin M, Bourke E, Alexander D, Warr MR, Barry-Holson K, Le Beau MM, Morrison CG, Passegué E. 2010. Hematopoietic stem cell quiescence promotes error-prone DNA repair and mutagenesis. Cell Stem Cell 7:174–185.

Nakachi K, Hayashi T, Hamatani K, Eguchi H, Kusunoki Y. 2008. Sixty years of follow-up of Hiroshima and Nagasaki survivors: Current progress in molecular epidemiology studies. Mutation Research 659:109–117.

Rongvaux A, Willinger T, Takizawa H, Rathinam C, Auerbach W, Murphy AJ, Valenzuela DM, Yancopoulos GD, Eynon EE, Stevens S, Manz MG, Flavell RA. 2011. Human thrombopoietin knockin mice efficiently support human hematopoiesis in vivo. Proceedings of the National Academy of Sciences of the USA 108: 2378–2383.

Rossi DJ, Jamieson CH, Weissman IL. 2008. Stems cells and the pathways to aging and cancer. Cell 132:681–696.

Rübe CE, Fricke A, Widmann TA, Fürst T, Madry H, Pfreundschuh M, Rübe C. 2011. Accumulation of DNA damage in hematopoietic stem and progenitor cells during human aging. PLoS One 6:e17487.

Srivastava N, Gochhait S, De Boer P, Bamezai RN. 2009. Role of H2AX in DNA damage response and human cancers. Mutation Research 681:180–188.

Takagi S, Saito Y, Hijikata A, Tanaka S, Watanabe T, Hasegawa T, Mochizuki S, Kunisawa J, Kiyono H, Koseki H, Ohara O, Saito T, Taniguchi S, Shultz LD, Ishikawa F. 2012. Membrane-bound human SCF/KL promotes in vivo human hematopoietic engraftment and myeloid differentiation. Blood 119:2768–2777.

Wang Y, Schulte BA, LaRue AC, Ogawa M, Zhou D. 2006. Total body irradiation selectively induces murine hematopoietic stem cell senescence. Blood 107:358–366.

Watson GE, Pocock DA, Papworth D, Lorimore SA, Wright EG. 2001. In vivo chromosomal instability and transmissible aberrations in the progeny of haemopoietic stem cells induced by high- and low-LET radiations. International Journal of Radiation Biology 77:409–417.

Yahata T, Takanashi T, Muguruma Y, Ibrahim AA, Matsuzawa H, Uno T, Sheng Y, Onizuka M, Ito M, Kato S, Ando K. 2011. Accumulation of oxidative DNA damage restricts the self-renewal capacity of human hematopoietic stem cells. Blood 118:2941–2950.

Int J Clin Exp Pathol 2013;6(1):76-79
www.ijcep.com /ISSN:1936-2625/IJCEP1209008

Original Article

Improved PCR amplification for molecular analysis using DNA from long-term preserved formalin-fixed, paraffin-embedded lung cancer tissue specimens

Masataka Taga[1*], Hidetaka Eguchi[1,2*], Tomoko Shinohara[1], Keiko Takahashi[1], Reiko Ito[1], Wataru Yasui[3], Kei Nakachi[1], Yoichiro Kusunoki[1], Kiyohiro Hamatani[1]

[1]Department of Radiobiology/Molecular Epidemiology, Radiation Effects Research Foundation; [2]Present address: Research Institute for Development Therapeutics & Translational Research Center, International Medical Center, Saitama Medical University; [3]Department of Molecular Pathology, Hiroshima University Graduate School of Biomedical Sciences, Hiroshima, Japan. [*]These authors contributed equally to this work.

Received September 13, 2012; Accepted October 26, 2012; Epub November 20, 2012; Published January 1, 2013

Abstract: Archival tissue specimens are valuable resources of materials for molecular biological analyses in retrospective studies, especially for rare diseases or those associated with exposure to uncommon environmental events. Although successful amplification with PCR is essential for analysis of DNA extracted from archival formalin-fixed, paraffin-embedded (FFPE) tissue specimens, we have often encountered problems with poor PCR amplification of target fragments. To overcome this, we examined whether heat treatment in alkaline solution could efficiently restore the PCR template activity of DNA that had already been extracted from FFPE lung cancer tissue specimens. The effect of the heat treatment was assessed by PCR for the *TP53* gene and other lung cancer-related gene loci. The heat treatment of DNA samples in borate buffer resulted in successful PCR amplification of DNA fragments ranging from 91 to 152 bp. This technique for restoration of template activity of DNA for PCR amplification is very simple and economical, and requires no special apparatus, so it may be applicable for molecular analysis of DNA samples from FFPE tissue specimens at various laboratories.

Keywords: FFPE, lung tissue specimen, DNA restoration, PCR

Introduction

Radiation Effects Research Foundation (RERF) has collected and stored a large number of archival formalin-fixed, paraffin-embedded (FFPE) tissue specimens obtained from atomic bomb (A-bomb) survivors. Archival tissue specimens have become valuable, especially for histological and molecular biological analyses of radiation-associated cancers in the case of RERF. Most of these specimens were fixed with formalin, embedded in paraffin and stored at room temperature, and DNA extracted from such specimens has been used as templates for PCR amplification. However, we have often had problems with poor PCR amplification, i.e., insufficient amounts of DNA functioned as template compared with intact DNA, and the limitations in amplifiable DNA size [1]. These issues can be attributable at least in part to DNA fragmentation and chemical modifications caused by fixation in formalin [2].

Recently, improvements of DNA isolation from FFPE tissue specimens were reported on the basis of the antigen retrieval principle [3, 4]. FFPE tissue specimens, without deparaffinization, were incubated in alkaline buffer at high temperatures (80-120°C) for 20 min, followed by phenol/chloroform treatment and ethanol precipitation, which resulted in higher yields and better quality of DNA in terms of PCR amplification. The key mechanism of action of heating in alkaline solution for DNA may be to denature and hydrolyze proteins, resulting in 1) rupture of cell and nuclear membranes and 2) breakage of cross-linkages caused by formalin fixation [3].

It was also reported that the chemical modification of bases of RNA by fixation in formalin can

Table 1. List of primers and PCR conditions

Gene or marker	Region	Primer sequence (5'- -3')	Annealing temperature (°C)	Mg^{2+} concentration (mM)	Extension temperature (°C)	Primer concentration (nM)	Size (bp)
TP53 (exon 8)	17p13	TGAGTAGTGGTA-ATCTACTGG	55	3 as $MgCl_2$	72	200	152
		TTGCTTACCTC-GCTTAGTGC					
TP53 (exon 7)	17p13	AGGTTGGCTCT-GACTGTACC	55	3 as $MgCl_2$	72	200	120
		CTCCTGACCTG-GAGTCTTCC					
D3S1266 (for *RARB*)	3p22-24	ACCTT-TATGGGAGT-GTCTTTGGGAGA	60	4 as $MgSO_4$	68	250	112
		TGGATG-GAAAANACGTAT-GTGTCTGTG					
D3S4614/Luca8.2 (for *RASSF1*)	3p21.3	GCTGAGAAATCT-CAATTGTGGGTG	58	3 as $MgCl_2$	72	500	126
		GGCTGCTGAG-CAGTGTCAGAC					
D3S4103 (for *FHIT*)	3p14.2	GCAGAG-CAAGACCCTATCT-CAT	60	2.5 as $MgSO_4$	68	500	91
		TGCCTTGGGTAG-ATTTATACCTG					
D9S171 (for *CDKN2A*)	9p21	CTCATCTCTGTCT-GCTGCCTCCT	59	3.5 as $MgSO_4$	68	250	109
		TTCTTGGGGC-TACTTTATTAA-CAATCA					

be partially removed by incubation in TE buffer (pH 7.0) [5] or citrate buffer (pH 4.0) [6] at 70°C, resulting in restoration of template activity for RT-PCR. Based on the notion that heat treatment in alkaline buffer can be usable for DNA already extracted from FFPE tissue specimens in order to restore template activity for PCR, we examined whether heat treatment of DNA which had already been extracted from FFPE lung cancer tissue specimens in alkaline solution could efficiently restore PCR amplification.

Materials and methods

Tissue specimens and DNA extraction

Subjects of this study comprised 11 lung cancer cases found in a Life Span Study cohort of A-bomb survivors. FFPE lung cancer tissue specimens from subjects who had undergone surgery at local hospitals in Hiroshima during 1987 - 2001 were obtained and unlinkably anonymized through the Study Group on Atomic Bomb Diseases, entrusted by the Ministry of Health, Labor and Welfare (MHLW) of Japan [7]. After deparaffinization of 5 μm sections using Hemo-De (Falma, Tokyo, Japan), the sections were stained with methylgreen (Sigma-Aldrich, St. Louis, MO) and dissected manually or by laser microdissection system AS LMD (Leica, Wetzler, Germany). DNA was extracted from microdissected tissue sections using QIAamp DNA Micro kit (QIAGEN, Hilden, Germany), according to the manufacturer's instruction.

This study was conducted under approval of the Genetic and Medical Ethics Commission at Hiroshima University, and the Human Investigation Committee and the Ethics Committee for Genome Research at RERF.

Heat treatment of DNA in borate buffer and PCR

Four hundred ng of DNA was heated in 100 μl of 25 mM citrate-acetate buffer (pH 5.0 or 6.0), 25 mM Tris-HCl buffer (pH 7.0 or 8.0) or 25 mM borate-NaOH buffer (pH 9.0, 10.0, or 11.0) at various temperatures (25-120°C) for 30 min, followed by ethanol precipitation in the pres-

A **Before DNA restoration**

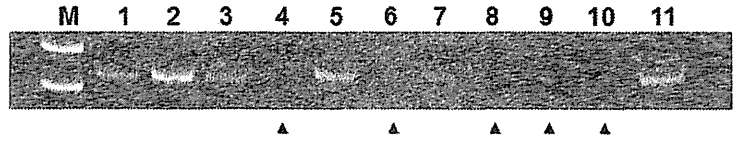

B **After DNA restoration**

C

Case #	Duration of storage (yrs)	PCR for					
		TP53 (exon 8)	*TP53* (exon 7)	D3S1266	D3S4614	D3S4103	D9S171
1*	14						
2*	15						
3*	18						
4	18						
5	17						
6	15						
7*	13						
8	12						
9	7						
10	4						
11*	4						

Figure 1. Improved PCR amplification by heating archival FFPE lung cancer tissue DNA in borate buffer. A: Polyacrylamide gel electrophoresis of PCR products (152 bp) for *TP53* (exon 8) using 10 ng of non-preheated DNA. Lane M is molecular size marker. Lanes 1-11 indicate PCR products of each lung cancer case. Closed arrow heads indicate cases with non-amplified DNA. B: PCR products amplified with 10 ng of preheated DNA. C: Summary of PCR amplification for *TP53* and lung cancer associated gene loci using non-preheated and preheated DNA. Empty grid indicates successful PCR using non-preheated DNA (in this case, PCR amplification using preheated DNA was not performed). Gray grid indicates successful PCR amplification using only preheated DNA. Black grid indicates no PCR amplification using either non-preheated or preheated DNAs. Cases with asterisks indicate successful PCR amplifications of all target fragments using 10 ng of non-preheated DNA.

ence of Ethachinmate (Nippon Gene, Tokyo, Japan) as carrier. Then, DNA was dissolved in TE buffer. As for PCR template, 10 ng of non-preheated or preheated DNA was used. PCR was performed using 0.5 U of Expand High Fidelity enzyme mixture (Roche Diagnostics, Basel, Switzerland) for *TP53*, 1 U of Platinum *Taq* DNA polymerase (Invitrogen, Carlsbad, CA) for D3S4614/Luca8.2, and 1 U of Platinum *Taq* DNA polymerase High Fidelity (Invitrogen) for D3S1266, D3S4103, and D9S171 in volume of 20 µl containing 1 x PCR buffer, 200-400 µM each of deoxyribonucleotide triphosphate mixture, Mg^{2+}, and each primer. PCR conditions consisted of initial denaturation (95°C for 2-3 min), followed by 44 cycles (40 cycles for *TP53*) of denaturation at 94°C for 30 sec, annealing for 1 min, extension for 30-60 sec, and a final extension for 7 min. Primer sets, temperatures of annealing and extension, and concentrations of Mg^{2+} are summarized in **Table 1**.

Results and discussion

Degraded DNA prepared from a colorectal cancer cell line, Colo210, that had been fixed with 15% unbuffered formalin for 3 days prior to DNA preparation, was used to preliminarily determine optimal conditions for heat treatment of DNA. As a result, preheating DNA to

100 or 120°C in buffer with pH 11 was most effective for PCR amplification (data not shown). To assess the effect of preheating DNA extracted from FFPE lung cancer tissue specimens on PCR amplification, DNA was incubated in borate buffer (pH 11.0) at 100°C for 30 min. PCR amplification of exon 8 in the *TP53* gene with 10 ng of preheated DNA indicated that the treatment had restored DNA template activity for PCR amplification in 4 of 5 samples (**Figure 1A and 1B**). Similar effects were observed in PCR amplification of several lung cancer-associated gene loci, summarized in **Figure 1C**. However, one case (#6) showed no effects of heat treatment on most of its PCR amplifications, possibly because conditions for fixation and/or storage of the tissue specimen were so severe that preheat treatment could not restore template activity of DNA. Furthermore, in two FFPE thyroid tissue specimens stored at RERF, PCR amplification of *TP53* with only 2.5 ng of preheated DNA produced DNA fragments longer than 200 bp, while 25 ng of non-preheated DNA was required for the same PCR amplification (data not shown).

These observations suggest that heat-treatment either during DNA extraction or after DNA extraction can restore DNA template activity for PCR amplification, although the extent of restoration depends on conditions of fixation and storage of tissue specimens. This improvement of PCR amplification may be due to the partial elimination of chemical modification of nucleic acids generated by fixation with formalin, as seen in heat-treatment of RNA from FFPE tissue specimens [5, 6].

This technique is very simple, cost-saving, and requires no special apparatus. We think it will be applicable for various molecular analyses of DNA samples from long-term preserved FFPE tissue specimens in general.

Acknowledgments

The Radiation Effects Research Foundation (RERF), Hiroshima and Nagasaki, Japan is a private, non-profit foundation funded by the Japanese Ministry of Health, Labour and Welfare (MHLW) and the U.S. Department of Energy (DOE), the latter in part through DOE Award DE-HS0000031 to the National Academy of Sciences. This publication was supported by RERF Research Protocols B35-04 and B37-04, and by JSPS Grant-in-Aid for Young Scientists (B) (21791238). The views of the authors do not necessarily reflect those of the two governments.

Conflict of interest statement

The authors have no conflicts of interest to disclose.

Address correspondence to: Dr. Masataka Taga, Department of Radiobiology/Molecular Epidemiology, Radiation Effects Research Foundation, 5-2 Hijiyama Park, Minami-ku, Hiroshima 732-0815, Japan. Tel: +81-82-261-3131; Fax: +81-82-261-3170; E-mail: taga@rerf.or.jp

References

[1] Iwamoto KS, Mizuno T, Ito T, Akiyama M, Takeichi N, Mabuchi K and Seyama T. Feasibility of using decades-old archival tissues in molecular oncology/epidemiology. Am J Pathol 1996; 149: 399-406.

[2] Srinivasan M, Sedmak D and Jewell S. Effect of fixatives and tissue processing on the content and integrity of nucleic acids. Am J Pathol 2002; 161: 1961-1971.

[3] Shi SR, Cote RJ, Wu L, Liu C, Datar R, Shi Y, Liu D, Lim H and Taylor CR. DNA extraction from archival formalin-fixed, paraffin-embedded tissue sections based on the antigen retrieval principle: heating under the influence of pH. J Histochem Cytochem 2002; 50: 1005-1011.

[4] Shi SR, Datar R, Liu C, Wu L, Zhang Z, Cote RJ and Taylor CR. DNA extraction from archival formalin-fixed, paraffin-embedded tissues: heat-induced retrieval in alkaline solution. Histochem Cell Biol 2004; 122: 211-218.

[5] Masuda N, Ohnishi T, Kawamoto S, Monden M and Okubo K. Analysis of chemical modification of RNA from formalin-fixed samples and optimization of molecular biology applications for such samples. Nucleic Acids Res 1999; 27: 4436-4443.

[6] Hamatani K, Eguchi H, Takahashi K, Koyama K, Mukai M, Ito R, Taga M, Yasui W and Nakachi K. Improved RT-PCR amplification for molecular analyses with long-term preserved formalin-fixed, paraffin-embedded tissue specimens. J Histochem Cytochem 2006; 54: 773-780.

[7] Yasui W and Oue N. Systematic collection of tissue specimens and molecular pathological analysis of newly diagnosed solid cancers among atomic bomb survivors. In: Shibata Y, Namba H, Suzuki K, Tomonaga M, editors. Radiation Risk Perspectives. Amsterdam: Elsevier. 2007. pp: 81-86.

THYROID
Volume 22, Number 11, 2012

DOI: 10.1089/thy.2011.0511

Rearranged Anaplastic Lymphoma Kinase (*ALK*) Gene in Adult-Onset Papillary Thyroid Cancer Amongst Atomic Bomb Survivors

Kiyohiro Hamatani,[1] Mayumi Mukai,[1] Keiko Takahashi,[1] Yuzo Hayashi,[2] Kei Nakachi,[1] and Yoichiro Kusunoki[1]

Background: We previously noted that among atomic bomb survivors (ABS), the relative frequency of cases of adult papillary thyroid cancer (PTC) with chromosomal rearrangements (mainly *RET/PTC*) was significantly greater in those with relatively higher radiation exposure than those with lower radiation exposure. In contrast, the frequency of PTC cases with point mutations (mainly $BRAF^{V600E}$) was significantly lower in patients with relatively higher radiation exposure than those with lower radiation exposure. We also found that among ABS, the frequency of PTC cases with no detectable gene alterations in *RET*, neurotrophic tyrosine kinase receptor 1 (*NTRK1*), *BRAF*, or *RAS* was significantly higher in patients with relatively higher radiation exposure than those with lower radiation exposure. However, in ABS with PTC, the relationship between the presence of the anaplastic lymphoma kinase (*ALK*) gene fused with other gene partners and radiation exposure has received little study. In this study, we tested the hypothesis that the relative frequency of rearranged *ALK* in ABS with PTC, and with no detectable gene alterations in *RET*, *NTRK1*, *BRAF*, or *RAS*, would be greater in those having relatively higher radiation exposures.
Methods: The 105 subjects in the study were drawn from the Life Span Study cohort of ABS of Hiroshima and Nagasaki who were diagnosed with PTC between 1956 and 1993. Seventy-nine were exposed (>0 mGy), and 26 were not exposed to A-bomb radiation. In the 25 ABS with PTC, and with no detectable gene alterations in *RET*, *NTRK1*, *BRAF*, or *RAS*, we examined archival, formalin-fixed, paraffin-embedded PTC specimens for rearrangement of *ALK* using reverse transcription–polymerase chain reaction and 5′ rapid amplification of cDNA ends (5′ RACE).
Results: We found rearranged *ALK* in 10 of 19 radiation-exposed PTC cases, but none among 6 patients with PTC with no radiation exposure. In addition, solid/trabecular-like architecture in PTC was closely associated with *ALK* rearrangements, being observed in 6 of 10 PTC cases with *ALK* rearrangements versus 2 of 15 cases with no *ALK* rearrangements. The six radiation-exposed cases of PTC harboring both *ALK* rearrangements and solid/trabecular-like architecture were associated with higher radiation doses and younger ages at the time of the A-bombing and at diagnosis compared to the other 19 PTC with no detectable gene alterations.
Conclusion: Our findings suggest that *ALK* rearrangements are involved in the development of radiation-induced adult-onset PTC.

Introduction

THYROID CANCER IS ONE OF THE MALIGNANCIES most closely associated with exposure to ionizing radiation in humans (1), such as the atomic-bombs in Hiroshima and Nagasaki and the Chernobyl nuclear power plant accident (2,3). Radiation Effects Research Foundation (RERF) epidemiology studies of atomic bomb survivors (ABS) have found that an excess relative risk for papillary thyroid cancer (PTC) per Gy is remarkably high among survivors (4,5). The data from the studies after the Chernobyl accident also indicate a strong relationship between thyroid cancer and radiation exposure (3).

Gene alterations that lead to constitutive activation of the mitogen-activated protein kinase (MAPK)-signaling pathway—such as alterations of *RET*, neurotrophic tyrosine kinase receptor 1 (*NTRK1*), *BRAF*, and *RAS* genes—are

[1]Department of Radiobiology/Molecular Epidemiology, Radiation Effects Research Foundation, Hiroshima, Japan.
[2]Geriatric Health Service Facility Hidamari, Hiroshima, Japan.

frequently found in PTC (6–8). These gene alterations can be detected in >70% of PTC cases, so the constitutive activation of the MAPK-signaling pathway appears to be a major early event in papillary thyroid carcinogenesis.

Our molecular analysis on rearrangements of *RET*, *NTRK1*, and *BRAF* genes, and also point mutations of *BRAF* and *RAS* genes in adult-onset PTC cases from the Life Span Study (LSS) cohort of ABS, found that the relative frequency of PTC cases with *RET/PTC* or *NTRK1* rearrangements (mainly *RET/PTC*) in all available PTC cases was significantly increased with an increased radiation dose, whereas PTC cases with *BRAF* or *RAS* point mutations (mainly $BRAF^{V600E}$) were significantly decreased (9,10). Apart from those PTC cases with known gene alterations, we found that the relative frequency of PTC cases with so-called nondetected gene alterations (i.e., no alterations in the *RET*, *NTRK1*, *BRAF*, or *RAS* gene) tended to increase with an increased radiation dose. The prevalence of the selected PTC cases peaked between 1956 and 1962, and rapidly decreased thereafter (10).

We postulated that some of the cases of PTC among ABS for which we had been unable to find gene alterations might have gene alterations that had previously not been looked for. Therefore, we initiated further molecular analyses of these cases by determining if some of them had rearrangements of anaplastic lymphoma kinase *(ALK)*.

The *ALK* gene was first identified as a fusion partner of nucleophosmin in anaplastic large-cell lymphoma (ALCL) with the t(2:5) chromosomal rearrangement (11,12). Translocation of *ALK* with multiple fusion partner genes was subsequently identified in ALCL as well as in other inflammatory myofibroblastic tumors (13). One novel type of *ALK* rearrangement was an echinoderm microtubule-associated protein-like 4 (*EML4*)-*ALK* fusion gene, which was recently detected in nonsmall-cell lung cancer (14). Numerous *EML4-ALK* fusion variants have been identified to date (15–18). The *EML4-ALK* fusion variants were also detected in breast and colon cancers (19), but to date, there has been no report on *ALK* rearrangements in thyroid cancer.

In this study, we report for the first time the finding that *ALK* rearrangement selectively occurred in radiation-exposed PTC cases that carried no known gene alterations, and that about half of the PTC cases with rearranged *ALK* developed solid/trabecular-like architecture in the cancer tissue. The PTC cases harboring both *ALK* rearrangements and solid/trabecular-like architecture were related to higher radiation doses and younger ages at the time of the bombings and at diagnosis compared to the other cases, implying a key role of *ALK* rearrangements in the development of radiation-induced thyroid cancer.

Methods

Study subjects and tissue specimens

The study subjects were 105 adults with PTC who were members of the LSS cohort of ABS of Hiroshima and Nagasaki diagnosed in selected hospitals in the two cities between 1956 and 1993. Of these, 79 were exposed (>0 mGy) and 26 were not exposed to A-bomb radiation. Of these 105 patients, 71 had been a part of our previous study on *RET/PTC* rearrangements (10). The 26 nonradiation-exposed subjects were either those with a radiation dose estimated to be 0 mGy or those who were not in the city of Hiroshima or Nagasaki at the time of the bombing. Study subjects who were not in these cities at the time of the bombing were assigned to the nonexposed group in this study, consistent with our previous article (10). This study was conducted with approval of the Human Investigation Committee and the Ethics Committee for Genome Research at the RERF.

Histological examination

Examination of histology was done by one of the authors (Y.H.) according to histopathological typing established by the WHO (20). All study specimens were nonbuffered, formalin-fixed, and paraffin-embedded PTC tissue specimens surgically resected from 1956 to 1993. Since amounts of tissue materials were limited, histological examination was conducted on one hematoxylin and eosin-stained tissue section per case.

RNA preparation and cDNA synthesis

RNA was extracted from microdissected noncancer or cancer regions using the High Pure RNA Paraffin Kit (Roche Diagnostics GmbH), as described previously (21). Reverse transcription was performed with random primers (9-mer) using 100 ng total RNA as template, as described previously (21).

Reverse transcription–polymerase chain reaction

Reverse transcription–polymerase chain reaction (RT-PCR) was carried out with the Fast Start High Fidelity PCR system (Roche Diagnostics GmbH) for the *ALK* gene, with AccuSure DNA polymerase (BIOLINE) for the *EML4* (exon 13)/*ALK* (exon 20) fusion and with Phusion Hot Start II (New England BioLabs) for the *EML4* (exon 20)/*ALK* (exon 20) fusion, using primer sets shown in Supplementary Table S1 (Supplementary Data are available online at www.liebertpub.com/thy) and as previously described (22).

Screening of rearranged ALK

The primer sets were made against the *ALK* kinase domain (K region) and the region spanning the boundary of exons 19 and 20 of *ALK* (W region) as shown in Figure 1A. PCR amplifications, for the K region with cDNA derived from 10 ng of total RNA of in-house control PTC and for the W region with cDNA from 5 ng of the same total RNA, were conducted at 36 cycles and 40 cycles, respectively. These PCR amplifications were repeated four times. The K/W ratios of 1.9 at 40 cycles or 2.9 at 36 cycles were drawn from an average of four experiments plus 2× the standard deviation as shown in Figure 1C. When the intensity ratio of the K region to W region after a 40-cycle RT-PCR amplification was >1.9 (Fig. 1B; samples II, III, and IV) based on the calculation shown in Figure 1C, samples were further analyzed by 36-cycle PCR amplification to determine whether the samples were positive for *ALK* rearrangements. We assumed that the samples with an intensity ratio >2.9 at 36-cycle PCR amplification were positive for *ALK* rearrangements (Fig. 1B; samples II, III, and IV). We used only the K/W ratio for screening, and intensities of individual amplified DNA fragments were not taken into account for screening the candidates. This screening was conducted only when clear and detectable K-region bands were observed in the first PCR products. Subsequently, cDNA fragments of

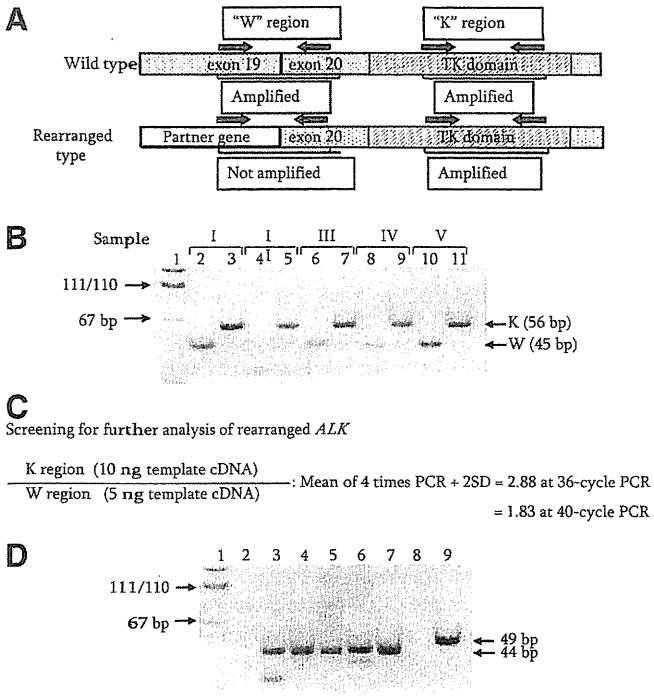

FIG. 1. **(A)** Diagram of the rearranged *ALK* gene. W and K regions indicate the regions spanning boundary of exons 19 and 20, and of exons 26 and 27 (kinase domain) in *ALK*, respectively. **(B)** Expression levels of W and K regions in *ALK*. The 5 μL of 40-cycle PCR products were electrophoresed on an 8% acrylamide gel. Sample I (lanes 2 and 3) indicates RT-PCR products of in-house control PTC. Samples II–V (lanes 4–11) reveal RT-PCR products of four exposed PTC with nondetected gene alterations; lanes with even numbers are cDNA fragments derived from the W region, and those with odd numbers are fragments derived from the K region. Lane 1 indicates pUC19-*Msp*I digest for DNA size marker. **(C)** Screening of the rearranged *ALK* gene. The intensity ratio for selection of rearranged *ALK* was calculated using RT-PCR amplification with cDNA derived from 10 ng of total RNA of in-house control PTC for the K region, and with cDNA derived from 5 ng of total RNA of the same PTC for the W region as template. **(D)** Detection of expression of *EML4-ALK* fusion genes by RT-PCR. Lanes 3–7 indicate cDNA fragments of the *EML4-ALK* fusion gene in PTC cases from which the 3′-end fragments of exon 13 of *EML4* were isolated by the SMART RACE method. Lanes 6 and 7 correspond to PTC in samples IV and III of **(B)**, respectively. Lane 9 indicates cDNA fragments (49 bp) derived from the chimera gene that was formed by fusion of exon 20 of *EML4* and exon 20 of *ALK*. Lanes 2 and 8 show H_2O for negative control, and Lane 1 shows pUC19-*Msp*I digest for DNA size marker. ALK, anaplastic lymphoma kinase; PTC, papillary thyroid cancer; RT-PCR, reverse transcription–polymerase chain reaction; RACE, rapid amplification of cDNA ends.

rearranged *ALK* genes were isolated and analyzed by the SMART rapid amplification of cDNA end (RACE) method, using primer sets shown in Supplementary Table S1 as described previously (22).

Statistical analysis

The Fisher's exact test was used for categorical variables. The Mann–Whitney *U* test was used for nonparametric two-sample comparison of continuous variables. SPSS software (version 15.0) was use for the statistical analyses. *p*-value was calculated by using a two-sided test. The Cochran-Armitage test for nonparametric trend analysis was carried out with Excel Statistics 2006 software.

Radiation dose

A-bomb radiation dose used in the analyses were shielded-organ doses to the thyroid as estimated by the recently implemented DS02 system (23), except for those cohorts who were not in the city of Hiroshima or Nagasaki at the time of the bombing.

Results

Detection of ALK *rearrangements in PTC cases with previously nondetected gene alterations*

Molecular epidemiological characteristics of 105 PTC cases examined thus far are shown in Supplementary Table S2, with 34 PTC cases that were newly added after our previous article (10). When comparing 79 radiation-exposed subjects and 26 nonexposed ones, no significant differences were found in distribution of gender, city, age at the time of the bombing (ATB), age at diagnosis, or presence or absence of *RET/PTC* rearrangements, *NTRK1* rearrangements, and *BRAF* or *RAS* point mutations. However, relative frequencies of *RET/PTC* rearrangements and *BRAF* mutation in radiation-exposed PTC cases showed significantly increasing or decreasing trends depending on the radiation dose ($P_{trend}=0.01$ and 0.0006), as shown in Supplementary Table S2. Furthermore, when comparing nonexposed PTC cases with those exposed to relatively a high radiation dose (the 3rd tertile, >355 mGy) for *RET/PTC* rearrangements, the relative frequency was significantly higher in exposed PTC cases (>355 mGy) than in nonexposed PTC cases (1/26 cases vs. 9/26 cases, respectively; $p=0.01$). On the other hand, the relative frequency of the *BRAF* mutation was significantly lower in PTC cases exposed to the radiation dose (>355 mGy) than in nonexposed PTC cases (19/26 cases vs. 7/26 cases, respectively; $p=0.002$). Among 105 PTC cases examined thus far for *RET*, *NTRK1*, and *BRAF* rearrangements and *BRAF* and *RAS* point mutations, 25 PTC cases were found to have no alterations in these genes, which tended to increase with an increased radiation dose, though this is not statistically significant (Supplementary Table S2). It should be noted that these cases showed a temporal change with a peak a short time after exposure, which then rapidly decreased (i.e., median time after exposure was 23 years for this group vs. 32 years for cases with *BRAF* and *RAS* point mutations, $p=0.014$). These findings are consistent with those in our previous article (10).

Of 25 PTC cases with previously nondetected gene alterations (also referred to as nondetected gene alterations) that carried no alterations in *RET*, *NTRK1*, *BRAF*, or *RAS* genes, we found *ALK* rearrangements in 10 of 19 radiation-exposed cases, but no *ALK* rearrangements in any of the six nonexposed cases (Table 1). The median dose in PTC cases with rearranged *ALK* was significantly higher than in grouped radiation-exposed and nonradiation-exposed PTC cases with no rearranged *ALK* (Fig. 2). However, there was no significant difference in the radiation dose between radiation-exposed PTC cases with rearranged *ALK* and with non-rearranged *ALK*. SMART 5′ RACE followed by sequencing analysis

TABLE 1. REARRANGED *ALK* IN PAPILLARY THYROID CANCER CASES WITH NONDETECTED GENE ALTERATIONS

	ALK rearrangements		
PTC case	*Present*	*Absent*	p[a]
Nonexposed ($n=6$)	0	6	0.051
Exposed (>0 mGy, $n=19$)	10[b]	9	

[a]Fisher's exact test.
[b]Five cases were *EML4*(exon 13)/*ALK*(exon 20); one case was *EML4*(exon 20)/*ALK*(exon 20); *ALK* partner genes in four cases have not been determined yet.
PTC, papillary thyroid cancer.

TABLE 2. ASSOCIATION BETWEEN REARRANGED *ALK* AND SOLID/TRABECULAR-LIKE ARCHITECTURE

	Rearranged *ALK*		
	Present (n=10)	*Absent* (n=15)	p[a]
Solid/trabecular-like architecture[b]			
Present	6[c]	2	0.028
Absent	4	13	

Data represent 25 PTC cases with nondetected gene alterations.
[a]Fisher's exact test.
[b]The samples were counted as positive for solid/trabecular-like architecture when that architecture was found in several areas within cancer regions.
[c]More than 50% of cancer regions revealed such architecture in two cases.

revealed that five PTC cases with rearranged *ALK* were a fusion of *EML4* (exon 13) and *ALK* (exon 20), and that one case was a fusion of *EML4* (exon 20) and *ALK* (exon 20) (Table 1). Expression of cDNA fragments of chimeric *EML4- ALK* in the PTC cases was confirmed by RT-PCR (Fig. 1D, lanes 3–7, and 9). The counterpart genes in the remaining four cases are currently being studied.

Morphological characteristics in PTC with rearranged ALK

Histological review of the10 PTC cases with rearranged *ALK* found that 6 of the10 had solid/trabecular-like architecture comprising either several small sites or several sites of greater total area within the cancer regions, but did not have insular architecture. Necrosis or mitotic figures were not observed in the single tissue section examined for each case. Supplementary Figure S1A and B show pathological photographs of two PTC cases with rearranged *ALK*, with solid/trabecular-like architecture in more than 50% of the cancers. Supplementary Figure S1C and D reveal a typical papillary structure for two exposed PTC cases with no rearranged *ALK*. In contrast, only 2 of 15 PTC cases with no rearranged *ALK* had such architecture. Analysis of 25 PTC cases with nondetected gene alterations revealed a close association between *ALK* rearrangement and solid/trabecular-like architecture ($p=0.028$, Table 2).

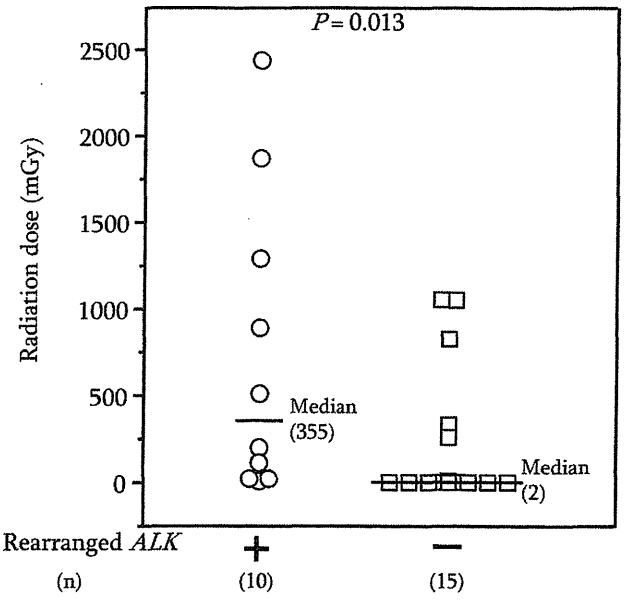

FIG. 2. Comparison of radiation dose distribution in PTC cases with (+, O) and without (−, □) rearranged *ALK*.

Association of PTC harboring both rearranged ALK *and solid/trabecular-like architecture with radiation dose and age at A-bombing*

Since there were only two PTC cases with no rearranged *ALK*, but having solid/trabecular-like architecture, we compared six PTC cases harboring both rearranged *ALK* and solid/trabecular-like architecture with the remaining 19 PTC cases in terms of radiation dose and ages at A-bombing and diagnosis (Fig. 3). These six PTC cases received significantly greater radiation doses and were or younger age at the time of A-bombing and at the time of diagnosis compared to the other 19 PTC cases (Fig. 3A–C, $p=0.005$, 0.008, and 0.016, respectively). Furthermore, comparison of 6 PTC cases harboring both rearranged *ALK* and solid/trabecular-like architecture with the remaining exposed 13 PTC cases by Mann–Whitney test also showed significant differences for radiation ($p=0.036$), age at A-bombing ($p=0.021$), and age at diagnosis ($p=0.020$).

Discussion

We report here the first evidence that rearrangements of *ALK* in adult-onset PTC cases develop in subjects exposed to radiation. Furthermore, the median radiation dose in PTC cases with rearranged *ALK* was significantly higher than in PTC cases with no rearranged *ALK* (Fig. 2), indicating involvement of rearranged *ALK* in radiation-induced papillary thyroid carcinogenesis. However, since only six nonexposed PTC cases were examined for rearranged *ALK*, it is necessary to examine a larger number of sporadic PTC cases to clarify possible presence of *ALK* rearrangements. We are thus unable at present to exclude the possibility that *ALK* rearrangements also occur in sporadic PTC. Although partner genes in four PTC cases have not yet been identified, PCR amplification in these cases was found in the K region, but not in the W region (Fig. 1), and therefore these PTC cases were judged to have rearranged *ALK*. We are attempting to identify the partner genes.

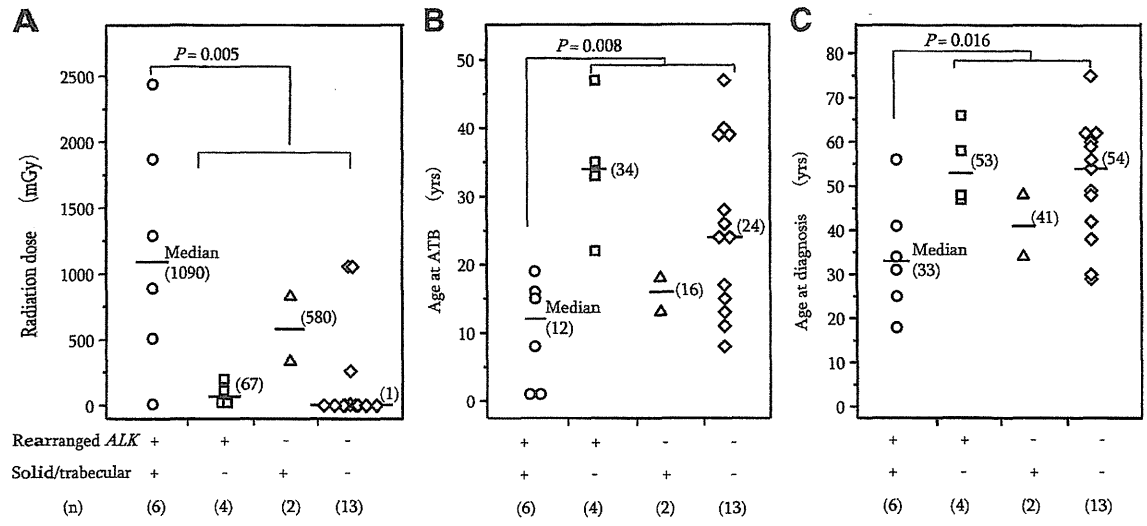

FIG. 3. Epidemiological characteristics of PTC cases harboring both the rearranged *ALK* gene and solid/trabecular-like architecture, in relation to radiation dose **(A)**, age at the time of atomic bombing **(B)**, and age at the time of diagnosis **(C)**.

Some of the 10 PTC cases with rearranged *ALK* revealed weak, but observable, PCR-amplified fragments as shown in Figure 1C. Those bands may be in part due to amplified fragments derived from another allele with wild-type *ALK*. Another plausible interpretation is that the rearrangement did not occur in all tumor cells. It is important to clarify whether *ALK* rearrangement is a driver mutation or a passenger mutation to better understand radiation-related carcinogenesis of PTC. Furthermore, although rearrangements of *ALK* are involved in the pathogenesis of many malignancies, including lymphoma and lung cancer, few *ALK* rearrangements have been well defined relative to their pathogenic role in cancer. Recently, constitutive *ALK* activation in several cancers was reported to cause the activation of selected downstream pathways, including MAPK and STAT (24,25), but no reports are available regarding a putative pathogenic role of rearranged *ALK* in PTC. To assess biological significance of rearranged *ALK* in radiation-induced PTC, *in vitro* and *in vivo* comparative experiments with *RET/PTC* rearrangements and *BRAF* point mutation need to be performed to shed light on these issues.

The nonradiation-exposed subjects in this study were comprised of two distinct groups: subjects whose radiation dose levels were estimated to be zero by the DS02 system, and subjects who were not in Hiroshima or Nagasaki, and thus not a part of the DS02 dose estimation. Our analyses included two not-in-city subjects in the six nonexposed subjects with nondetected gene alterations, but even when we excluded these not-in-city subjects from the analysis, the results were substantially unchanged. Specifically, the six nonexposed subjects without rearranged *ALK* in Table 1 would become 4 ($p = 0.1$ in this case); the median value of 2 mGy for 15 subjects with no rearranged *ALK* in Figure 2 would become 3 mGy for 13 subjects ($p = 0.034$); and the 13 subjects (denoted by "◇") in Figure 3 harboring neither rearranged *ALK* nor solid/trabecular-like architecture would become 11, and their median values of 1 mGy, 24 years, and 54 years in Figure 3A–C would be 2 mGy, 24 years, and 54 years ($p = 0.009$, 0.012, and 0.023), respectively.

The solid/trabecular-like architecture appeared in one of three different types of groupings as (I) relatively small, clonal, multicellular clusters distributed throughout the cancer; (II) larger groupings (each composed of a few multicellular clusters) distributed throughout the cancer, or as (III) a few large groupings that occupied a major portion (>50%) of the cancer volume. Interestingly, 6 of 10 PTC cases with rearranged *ALK* had solid/trabecular-like architecture corresponding to types (I) and (II) above (numbering 3 and 1, respectively) in several areas within the cancers, and two cases had such architecture in more than 50% of the cancer (type III and shown in Supplementary Fig. 1A, B). However, only 2 of 15 PTC cases with no rearranged *ALK* had such architecture; they were small and found in several areas scattered throughout the cancer (type I). The 25 PTC cases with nondetected gene alterations showed no necrosis or mitotic figures, but did show PTC-specific nuclear features such as nuclear groves, intranuclear cytoplasmic inclusions, and psammoma bodies. Taking into account the diagnostic criteria proposed by Volante *et al.* (26), it is reasonable to conclude that two PTC cases harboring solid/trabecular-like architecture in more than 50% of cancer regions are a mixed type of PTC and solid variant, or a solid variant of PTC rather than poorly differentiated thyroid cancer. This is true even though the size of one solid/trabecular nest was small and uniform compared with that of post-Chernobyl childhood PTC, and that the other six PTC cases (four and two with and without rearranged *ALK*, respectively) harboring such architecture in several cancer regions are typical PTC.

PTC cases harboring both rearranged *ALK* and solid/trabecular-like architecture were significantly associated not only with a greater radiation dose but also with younger age at the time of bombing and at diagnosis, compared with the remaining PTC cases. One plausible interpretation of this finding is that in the process of radiation-induced papillary thyroid carcinogenesis involving *ALK* rearrangements, unknown gene alterations may additionally occur and generate solid/trabecular-like architecture. Considering this, further analysis will be required to identify such gene alterations and

to assess the pathogenic role of *ALK* rearrangements and its potential link to solid/trabecular-like architecture.

Acknowledgments

The RERF, Hiroshima and Nagasaki, Japan, is a private, nonprofit foundation funded by Japan's Ministry of Health, Labour, and Welfare, and the U.S. Department of Energy (DOE), the latter in part through DOE Award DE-HS0000031 to the National Academy of Sciences. This publication was supported by RERF Research Protocols RP 5-02, and in part by a Grant-in-Aid for Science Research from the Ministry of Education, Culture, Sports, Science, and Technology, and a Grant-in Aid for Cancer Research from Japan's Ministry of Health, Labour, and Welfare, as well as research grant for the Princess Takamatsu Cancer Research Fund (08-24015). We thank Dr. J. Cologne for his helpful statistical advice, Mr. K. Koyama for his excellent technical assistance, and Ms. M. Yonezawa for her good help with preparation of article. The views of the authors do not necessarily reflect those of the two governments.

Disclosure Statement

The authors declare that they have no commercial associations that might create a conflict of interest in connection with this article.

References

1. Imaizumi M, Usa T, Tominaga T, Neriishi K, Akahoshi M, Nakashima E, Ashizawa K, Hida A, Soda M, Fujiwara S, Yamada M, Ejima E, Yokoyama N, Okubo M, Sugino K, Suzuki G, Maeda R, Nagataki S, Eguchi K 2006 Radiation dose-relationships for thyroid nodules and autoimmune thyroid diseases in Hiroshima and Nagasaki atomic bomb survivors 55–58 years after radiation exposure. JAMA **295:** 1011–1022.
2. Kazakov VS, Demidchik EP, Astakhova LN 1992 Thyroid cancer after Chernobyl. Nature **359:**21.
3. Astakhova LN, Anspaugh LR, Beebe G.W, Bouville A, Drozdovitch VV, Garber V, Gavrilin YI, Khrouch VT, Kuvshinnikov AV, Kuzmenkov YN, Minenko VP, Moschik KV, Nalivko AS, Robbins J, Shemiakina EV, Shinkarev S, Tochitskaya SI, Waclawiw MA 1998 Chernobyl-related thyroid cancer in children of Belarus: A case-control study. Radiat Res **150:**349–356.
4. Thompson DE, Mabuchi K, Ron E, Soda M, Tokunaga M, Ochikubo S, Sugimoto S, Ikeda T, Terasaki M, Izumi S, Preston DL 1994 Cancer incidence in atomic bomb survivors. Part II: Solid tumors, 1958–1987. Radiat Res **137:**S17–S67.
5. Preston DL, Ron E, Tokuoka S, Funamoto S, Nishi N, Soda M, Mabuchi K, Kodama K 2007 Solid cancer incidence in atomic bomb survivors: 1958–1998. Radiat Res **168:**1–64.
6. Gandhi M, Evdokimova V, Nikiforov YE 2010 Mechanisms of chromosomal rearrangements in solid tumors: the model of papillary thyroid carcinoma. Mol Cell Endcrinol **321:**36–43.
7. Greco A, Miranda C, Pierotti MA 2010 Rearrangements of *NTRK1* gene in papillary thyroid carcinoma. Mol Cell Endocrinol **321:**44–49.
8. Xing M 2010 Prognostic utility of *BRAF* mutation in papillary thyroid cancer. Mol Cell Endocrinol **321:**86–93.
9. Takahashi K, Eguchi H, Arihiro K, Ito R, Koyama K, Soda M, Cologne J, Hayashi Y, Nakata Y, Nakachi K, Hamatani K 2007 The presence of *BRAF* point mutaion in adult papillary thyroid carcinomas from atomic bomb survivors correlates with radiation dose. Mol Carcinog **46:**242–248.
10. Hamatani K, Eguchi E, Ito R, Mukai M, Takahashi K, Taga M, Imai K, Cologne J, Soda M, Arihiro K, Fujihara M, Abe K, Hayashi T, Nakashima M, Sekine I, Yasui W, Hayashi Y, Nakachi K 2008 *RET/PTC* rearrangements preferentially occurred in papillary thyroid cancer among atomic bomb survivors exposed to high radiation dose. Cancer Res **68:** 7176–7182.
11. Morris SW, Kirstein MN, Valentine MB, Dittmer KG, Shapiro DN, Saltman DL, Look AT 1994 Fusion of a kinase gene, ALK, to a nucleolar protein gene, NPM, in non-Hodgkin's lymphoma. Science **263:**1281–1284.
12. Shiota M, Fujimoto J, Tanegawa M, Satoh H, Ichinohasama R, Abe M, Nakano M, Yamamoto T, Mori S 1994 Diagnosis of t(2;5)(p23;q35)-associated Ki-1 lymphoma with immunohistochemistry. Blood **84:**3648–3652.
13. Pulford K, Morris SW, Turturro F 2004 Anaplastic lymphoma kinase proteins in growth control and cancer. J Cell Physiol **199:**330–358.
14. Soda M, Choi YL, Enomoto M, Takada S, Yamashita Y, Ishikawa S, Fujiwara S, Watanabe H, Kurashina K, Hatanaka H, Bando M, Ohno S, Ishikawa Y, Aburatani H, Niki T, Sohara Y, Sugiyama Y, Mano H 2007 Identification of the transforming *EML4-ALK* fusion gene in non-small-cell lung cancer. Nature **448:**561–566.
15. Mano H 2008 Non-solid oncogenes in solid tumors: *EML4-ALK* fusion genes in lung cancer. Cancer Sci **99:** 2349–2355.
16. Choi YL, Takeuchi K, Soda M, Inamura K, Togashi Y, Hatano S, Enomoto M, Hamada T, Haruta H, Watanabe H, Kuruhashi K, Hatanaka H, Ueno T, Takda S, Yamashita Y, Sugiyama Y, Ishikawa Y, Mano H 2008 Identification of novel isoforms of the *EML4-ALK* transforming gene in non-small cell lung cancer. Cancer Res **68:**4971–4976.
17. Takeuchi K, Choi YL, Soda M, Inamura K, Togashi Y, Hatano S, Enomoto M, Takada S, Yamashita Y, Satoh Y, Okumura S, Nakagawa K, Ishikawa Y, Mano H 2008 Multiplex reverse transcription-PCR screening for *EML4-ALK* fusion transcripts. Clin Cancer Res **14:**6618–6624.
18. Takeuchi K, Choi YL, Togashi Y, Soda M, Hanata S, Inamura K, Takada S, Ueno T, Yamashitaa Y, Satoh Y, Okumura S, Nakagawa K, Ishikawa Y, Mano H 2009 KIF5B-ALK, a novel fusion oncokinase identified by an immunohistochemistry-based diagnostic system for ALK-positive lung cancer. Clin Cancer Res **15:**3143–3149.
19. Lin E, Li L, Guan Y, Soriano R, Rivers CS, Mohan S, Pandita A, Tang J, Modrusan Z 2009 Exon array profiling detects *EML4-ALK* fusion in breast, colorectal, and non-small cell lung cancers. Mol Cancer Res **7:**1466–1476.
20. DeLellis RA, Lloyd RV, Heitz PU, Eng C (eds) 2004 World Health Organization Classification of Tumours. Pathology and Genetics of Tumours of Endocrine Organs. IARC Press, Lyon, France.
21. Hamatani K, Eguchi H, Takahashi K, Koyama K, Mukai M, Ito R, Taga M, Yasui W, Nakachi K 2006 Improved RT-PCR amplification for molecular analyses with long-term preserved formalin-fixed, paraffin-embedded tissue specimens. J Histochem Cytochem **54:**773–780.
22. Hamatani K, Eguchi H, Mukai M, Koyama K, Taga M, Ito R, Hayashi Y, Nakachi K 2010 Improved methods for analysis of RNA present in long-term preserved thyroid cancer tissue of atomic bomb survivors. Thyroid **20:**43–49.

23. Young RW, Kerr GD (eds) 2005 Reassessment of the Atomic Bomb Radiation Dosimetry for Hiroshima and Nagasaki Dosimetry System 2002. Radiation Effects Research Foundation, Hiroshima, Japan.
24. Chiarle R, Voena C, Ambrogio C, Piva R, Inghirami G 2008 The anaplastic lymphoma kinase in the pathogenesis of cancer. Nat Rev Cancer **8**:11–23.
25. Shaw ST, Solomon B 2011 Targeting anaplastic lymphoma kinase in lung cancer. Clin Cancer Res **17**:2081–2086.
26. Volante M, Collini P, Nikiforov YE, Sakamoto A, Kakudo K, Katoh R, Lloyd RV, LiVolsi VA, Papotti M, Sobrinho-Simoes M, Bussolati G, Rosai J 2007 Poorly differentiated thyroid carcinoma: the Turin proposal for the use of uniform diagnostic criteria and an algorithmic diagnostic approach. Am J Sug Pathol **31**:1256–1264.

Address correspondence to:
Kiyohiro Hamatani, Ph.D.
Department of Radiobiology/Molecular Epidemiology
Radiation Effects Research Foundation
5-2 Hijiyama Park
Minami-ku
Hiroshima 732-0815
Japan

E-mail: hamatani@rerf.or.jp

IJC
International Journal of Cancer

Stroma-directed imatinib therapy impairs the tumor-promoting effect of bone marrow-derived mesenchymal stem cells in an orthotopic transplantation model of colon cancer

Kei Shinagawa[1], Yasuhiko Kitadai[1], Miwako Tanaka[1], Tomonori Sumida[1], Mieko Onoyama[1], Mayu Ohnishi[1], Eiji Ohara[1], Yukihito Higashi[2], Shinji Tanaka[3], Wataru Yasui[4] and Kazuaki Chayama[1]

[1] Department of Gastroenterology and Metabolism, Graduate School of Biomedical Sciences, Hiroshima University, Hiroshima, Japan
[2] Department of Cardiovascular Physiology and Medicine, Graduate School of Biomedical Sciences, Hiroshima University, Hiroshima, Japan
[3] Department of Endoscopy, Hiroshima University Hospital, Hiroshima, Japan
[4] Department of Molecular Pathology, Graduate School of Biomedical Sciences, Hiroshima University, Hiroshima, Japan

Bone marrow-derived mesenchymal stem cells (MSCs) are reported to contribute to formation of tumor-promoting stromal cells. We reported recently that, in an orthotopic nude mice model of colon cancer, MSCs traveled to tumor stroma, where they differentiated into carcinoma-associated fibroblast (CAF)-like cells. We also found that CAFs express platelet-derived growth factor receptor (PDGFR) at a high level and that imatinib therapy targeting PDGFR in CAFs inhibits growth and metastasis of human colon cancer. These findings led us to examine whether the tumor-promoting effect of MSCs is impaired by blockade of PDGFR signaling achieved with imatinib. Orthotopic transplantation and splenic injection of human MSCs along with KM12SM human colon cancer cells, in comparison with transplantation of KM12SM cells alone, resulted in significantly greater promotion of tumor growth and liver metastasis. The KM12SM + MSC xenograft enhanced cell proliferation and angiogenesis and inhibited tumor cell apoptosis. When tumor-bearing animals were treated with imatinib, there was no significant increase in primary tumor volume or total volume of liver metastases, despite the KM12SM+MSC xenograft, and survival in the mixed-cell group was prolonged by imatinib treatment. Moreover, the ability of MSCs to migrate to tumor stroma was impaired, and the number of MSCs surviving in the tumor microenvironment was significantly decreased. In *in vitro* experiments, treatment with imatinib inhibited migration of MSCs. Our data suggest that blockade of PDGF signaling pathways influences the interaction between bone marrow-derived MSCs and tumor cells in the tumor microenvironment and, hence, inhibits the progressive growth of colon cancer.

Key words: mesenchymal stem cells, carcinoma-associated fibroblasts, orthotopic colon cancer model, platelet-derived growth factor receptor, imatinib

Abbreviations: CAF: carcinoma-associated fibroblast; DAPI: 4′,6-diamidino-2-phenylindole; DMEM: Dulbecco's Modified Eagle's Medium; FBS: fetal bovine serum; HBSS: Hanks' balanced salt solution; MSC: mesenchymal stem cell; MVA: microvessel area; PCNA: proliferating cell nuclear antigen; PCNA-LI: PCNA labeling index; PDGF: platelet-derived growth factor; PDGFR: platelet-derived growth factor receptor

Grant sponsors: Grants-in-Aid for Cancer Research from the Ministry of Education, Culture, Science, Sports and Technology of Japan, Ministry of Health, Labor and Welfare of Japan
DOI: 10.1002/ijc.27735
History: Received 12 Oct 2011; Accepted 28 Jun 2012; Online 23 Jul 2012

Correspondence to: Yasuhiko Kitadai, Department of Gastroenterology and Metabolism, Graduate School of Biomedical Sciences, Hiroshima University, 1-2-3 Kasumi, Minami-Ku, Hiroshima 734-8551, Japan, Tel.: +81-82-257-5191, Fax: +81-82-257-5194, E-mail: kitadai@hiroshima-u.ac.jp

Many recent reports have referred to tumor-stromal interactions as essential events for tumor progression.[1–3] Of the constituents of tumor stroma, it has become clear that activated fibroblasts, called carcinoma-associated fibroblasts (CAFs), promote tumor growth and metastasis.[4–8] We previously reported that the platelet-derived growth factor (PDGF)/PDGF receptor (PDGFR) signaling pathway plays a critical role in the growth and metastasis of gastric and colon cancers in orthotopic transplantation models.[4,8] Tumor cells express PDGFs, and PDGFRs are expressed by CAFs. The origin of CAFs is not fully understood, but they may arise from fibroblasts residing in local tissues,[7] periadventitial cells including pericytes and vascular smooth muscle cells,[9] endothelial cells,[10] and bone marrow-derived cells including various stem cells.[11]

Mesenchymal stem cells (MSCs) can be recruited from bone marrow to inflamed or damaged tissues by local endocrine signals, resulting in tissue regeneration.[12,13] Although MSCs are known to migrate to a variety of tumors, such as melanomas,[14] gliomas,[15,16] and colon,[17,18] pancreatic,[19,20] and breast cancers,[21–23] the mechanisms of the migratory effect are very complex, and the key factors have not been identified. Experimental co-injection of tumor cells and MSCs has revealed

What's new?
Platelet-derived growth factor (PDGF) signaling pathways are crucial for the migration of metastasis-promoting mesenchymal stem cells (MSCs) to the tumor microenvironment in human colon cancer. In this study employing orthotopic transplantation of human MSCs and colon cancer cells in mice, inhibition of PDGF signaling with the drug imatinib was found to influence interactions between bone marrow-derived MSCs and tumor cells, suggesting that stroma-directed imatinib therapy could be effective against colon cancer progression.

that MSCs promote tumor growth and metastasis[22,24–33] and are implicated in tumor invasion and angiogenesis,[17,24,30,31] immunosuppression,[25,26] inhibition of apoptosis,[29] and formation of a cancer stem cell niche.[32] Our recent study showed that MSCs accumulating in the tumor microenvironment differentiate into CAFs and promote growth and metastasis of colon cancer.[34] Very recently, it was shown in a mouse model of gastric cancer that at least 20% of CAFs originate from bone marrow-derived MSCs.[35] PDGF signaling pathways are known to be crucial to migration and survival of MSCs.[15,19,36]

In an orthotopic transplantation model of human colon cancer, we examined the effect of imatinib, known to be a potent tyrosine kinase inhibitor of PDGFR,[37] on migration and survival of MSCs in the tumor microenvironment and on promotion of tumor growth and metastasis by MSCs. We found that treatment with imatinib inhibited tumor-MSC interactions and modified tumor-supporting stroma.

Material and Methods

Cell culture

Human MSCs were harvested from the iliac crest and isolated and cultured according to a protocol approved by the Ethics Committee of Hiroshima University Graduate School of Medicine, as described previously.[34,38] The capacity for chondrogenic, adipogenic, and osteogenic differentiation was confirmed with the use of a Human Mesenchymal Stem Cell Functional Identification Kit (R&D Systems, Minneapolis, MN). Cell surface antigens on the MSCs were analyzed by fluorescence-activated cell sorting, and it was confirmed that the cells were positive for CD29, CD44, CD73, CD90, CD105, CD166, and MHC-DR but negative for CD14, CD34, and Flk-1, as described previously.[38] MSCs were fluorescently labeled with red fluorescent linker dye (PKH26 Red Fluorescent Cell Linker Kit; Sigma, Sigma-Aldrich, St Louis, MO) according to the manufacturer's instructions.

Human colon cancer cell line KM12SM[39] was kindly gifted by Dr. Isaiah J. Fidler (University of Texas). Cells were maintained in DMEM supplemented with 10% fetal bovine serum (FBS), L-glutamine, and a penicillin-streptomycin solution. The cultures were maintained for no longer than 12 weeks after recovery of cells from frozen stock.

Animals and transplantation of tumor cells

Female athymic BALB/c nude mice were obtained from Charles River Japan (Tokyo, Japan). The mice were maintained under specific pathogen-free conditions and used at 8 weeks of age. The study was carried out after permission was granted by the Committee on Animal Experimentation of Hiroshima University.

To produce cecal tumors, KM12SM cells in 50 μL of Hanks' balanced salt solution (HBSS) were injected into the cecal wall of nude mice under observation with a zoom stereomicroscope. To produce experimental liver metastases, the cells were injected into the spleen of nude mice as described previously.[39]

Anticancer drug

Imatinib (imatinib mesylate or Gleevec; Novartis Pharma AG, Basel, Switzerland) was diluted in sterile water for administration by oral gavage.

Effect of imatinib on tumor tropism of MSCs in vivo

Because we have found that MSCs migrate to orthotopic and metastatic tumor sites,[34] we examined whether imatinib affects the tumor tropism of MSCs. We injected 0.5×10^6 KM12SM cells into the cecal wall in six mice on day 0. One week after the orthotopic implantation of tumor cells (on day 7), mice were randomized into two groups: one given water daily (control group) and the other given 50 mg/kg/day imatinib by oral gavage once daily until day 28. Three weeks after tumor cell transplantation (on day 21), each mouse was injected with 1.0×10^6 PKH26-labeled MSCs (in 200 μL of HBSS) in the tail vein. One week after this injection (on day 28), the mice were killed and necropsied.

KM12SM cells (0.5×10^6) were transplanted into the spleen of six additional mice on day 0. One week after tumor cell transplantation (on day 7), mice were randomized into two groups: one given water daily (control group) and the other given 50 mg/kg/day imatinib by oral gavage once daily until day 28. At the same time (on day 7), each mouse was injected with 1.0×10^6 PKH26-labeled MSCs (in 200 μL of HBSS) in the tail vein. Three weeks after this injection (on day 28), the mice were killed.

Necropsy procedures and histologic studies

Mice bearing orthotopic tumors were killed with an overdose of methophane. Necropsy was performed, after which tumors were excised and measured. For immunohistochemical and hematoxylin and eosin (H&E) staining, one part of the tumor tissue was fixed in formalin-free IHC Zinc Fixative (PharMingen, San Diego, CA) and embedded in paraffin, and the

other part was embedded in OCT compound (Sakura Finetek Japan, Tokyo, Japan), rapidly frozen in liquid nitrogen, and stored at −80°C. Sections of PKH26-labeled tissues were analyzed by means of fluorescence confocal microscopy.

Effect of imatinib on interactions between tumor cells and MSCs in orthotopic colon tumor

To examine the effect of imatinib on the tumor-MSC interactions in orthotopic colon tumors, co-injection studies were carried out. Mice were divided into four groups according to the kind(s) of implanted cells and the treatment received: (*i*) KM12SM cells alone and daily administration of water by oral gavage (0.5×10^6, $n = 19$), (*ii*) KM12SM cells mixed with MSCs and daily administration of water by oral gavage (KM12SM:MSC ratio, 0.5×10^6:1.0×10^6 [1:2]; $n = 21$), (*iii*) KM12SM cells alone and daily oral gavage 50 mg/kg imatinib (0.5×10^6, $n = 8$), or (*iv*) KM12SM cells mixed with MSCs and daily oral gavage 50 mg/kg imatinib [KM12SM:MSC ratio, 0.5×10^6:1.0×10^6, [1:2]; $n = 12$).

Treatment with imatinib was begun 1 week after intracecal transplantation of cells and lasted 5 weeks. Surviving mice were then killed and necropsied [(*i*) $n = 18$, (*ii*) $n = 10$, (*iii*) $n = 8$, (*iv*) $n = 10$]. Tumor volume, incidence of liver metastasis, and survival were evaluated. Tumor volume (V) was calculated as $V = (1/2)ab^2$, where a is the largest diameter of the tumor and b is the smallest diameter.

Quantification of the remaining MSCs and phosphorylation of PDGFR-β in MSCs coimplanted with tumor cells in vivo

To evaluate how many MSCs coimplanted with tumor cells remained at the orthotopic tumor site, and whether PDGFR-β in MSCs was phosphorylated, KM12SM cells mixed with PKH26-labeled MSCs (0.5×10^6:1.0×10^6 [1:2]) were injected into the cecal wall in three mice. Three weeks after intracecal transplantation, tumors were excised and analyzed by means of fluorescence confocal microscopy to detect PKH26-labeled MSCs and to confirm phosphorylation of PDGFR-β in MSCs by immunofluorescence staining as described previously.[34] For quantification of the remaining MSCs, 10 random fields were captured with a 20× objective lens, and red fluorescence areas were measured. The areas were calculated with the use of NIH ImageJ software.

Effect of imatinib on interactions between tumor cells and MSCs in a liver metastasis model

To evaluate the effect of imatinib on the tumor-MSC interactions in liver metastases, we developed a model of liver metastasis by injecting tumor cells into mice spleen as described previously.[39] Mice were divided into four groups according to the kind(s) of implanted cells and the treatment received ($n = 10$ in each group): (*i*) KM12SM cells alone and daily administration of water by oral gavage (0.5×10^6), (*ii*) KM12SM cells mixed with PKH26-labeled MSCs and daily administration of water by oral gavage (KM12SM:PKH26-labeled MSC ratio, 0.5×10^6:1.0×10^6 [1:2]), (*iii*) KM12SM cells alone and daily oral gavage 50 mg/kg imatinib (0.5×10^6), (*iv*) KM12SM cells mixed with PKH26-labeled MSCs and daily oral gavage 50 mg/kg imatinib (KM12SM:PKH26-labeled MSCs, 0.5×10^6:1.0×10^6 [1:2]).

One week after intrasplenic transplantation of cells, mice were treated with imatinib for 3 weeks; surviving mice were then killed and necropsied ($n = 10$ in each group). Tumor nodules on the liver surface were counted macroscopically. Metastatic tumors were analyzed by means of fluorescence confocal microscopy to detect PKH26-labeled MSCs.

Antibodies

Rabbit anti-PDGFR-β and rabbit antiphosphorylated PDGFR-β (p-PDGFR-β) (Santa Cruz Biotechnology, Santa Cruz, CA), mouse antiproliferating cell nuclear antigen (PCNA) (Dako, Glostrup, Denmark), and rat anti-mouse CD31 (BD Pharmingen, San Diego, CA) were used as primary antibodies. Biotinylated rabbit anti-rat IgG (Dako) and biotinylated goat anti-mouse IgG (Dako) were used as secondary antibodies. Alexa Fluor® 488-labeled goat anti-rabbit IgG (Invitrogen, Carlsbad, CA) was used as fluorescent secondary antibody.

Immunohistochemical determination of PCNA, apoptotic cells, and microvessel area (MVA)

Paraffin-embedded tissues cut into 4 μm sections and frozen tissues cut into 8 μm sections were used for immunohistochemical identification of PCNA and CD31, respectively. Immunohistochemistry was performed as described previously.[40] The PCNA labeling index (PCNA-LI) was taken as the ratio of positively stained tumor cells to the total tumor cells and expressed as a percentage for each case.[34] Apoptotic cells in paraffin sections of KM12SM tumors were detected by terminal deoxynucleotide transferase-mediated dUTP-biotin nick end labeling with the ApopTag Plus Peroxidase In Situ Apoptosis Detection Kit (Chemicon, Temecula, CA) according to the manufacturer's instructions. The apoptotic index (AI) was taken as the ratio of positively stained tumor cells and apoptotic bodies to all tumor cells and expressed as a percentage for each case.[34] Angiogenic activity was evaluated according to the areas of microvessels stained with anti-mouse CD31 antibody. For quantification of the MVA, 10 random fields at 100× magnification were captured for each tumor, and the outline of each microvessel including a lumen was manually traced. The area was then calculated with the use of NIH ImageJ software.

Confocal microscopy

Confocal fluorescence images were captured with a 20× or 40× objective lens on a Zeiss LSM 510 laser scanning microscopy system (Carl Zeiss Inc., Thornwood, NY) equipped with a motorized Axioplan microscope, argon laser (458/477/488/514 nm, 30 mW), HeNe laser (543 nm, 1 mW), HeNe laser (633 nm, 5 mW), LSM 510 control and image acquisition software, and appropriate filters (Chroma Technology Corp., Brattleboro, VT). Confocal images were exported to Adobe Photoshop software, and image montages were prepared.

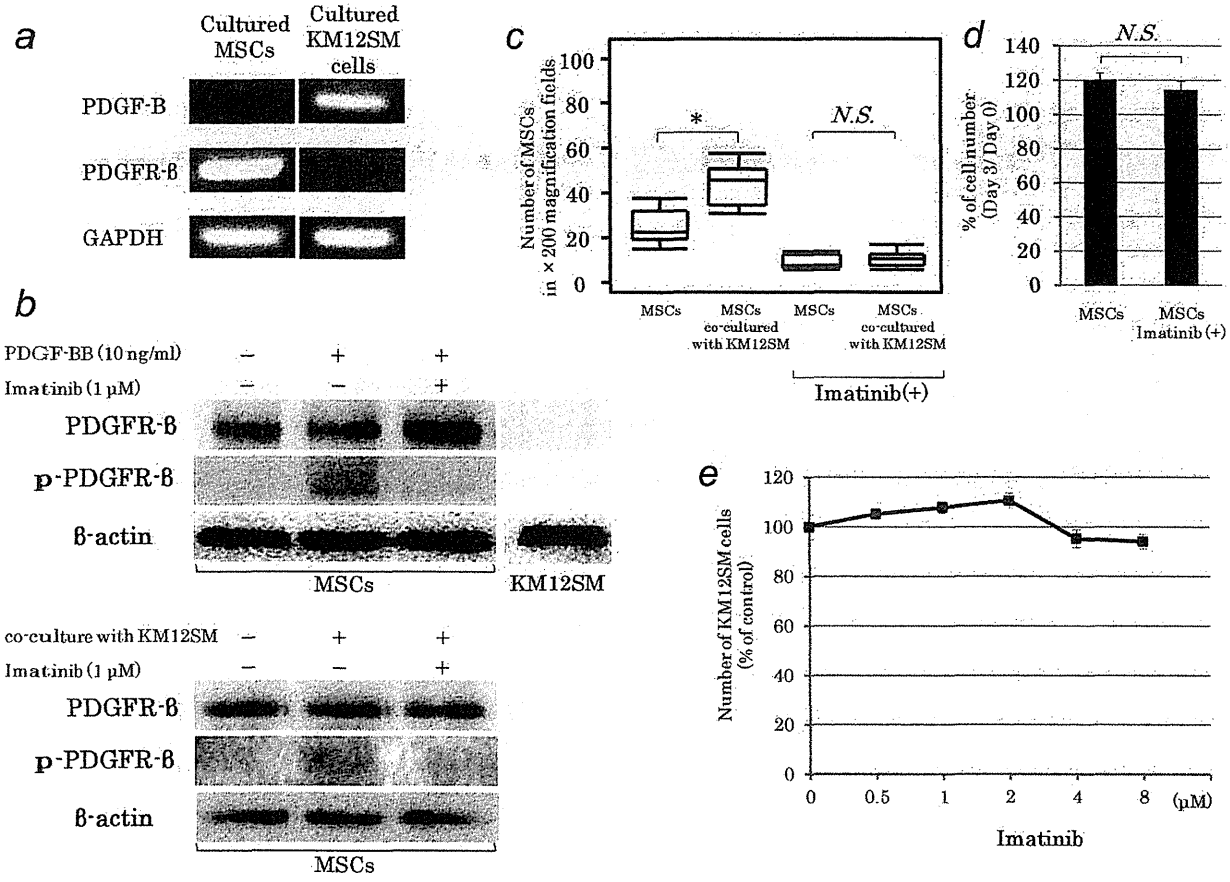

Figure 1. Effect of imatinib on KM12SM cells and MSCs *in vitro*. (*a*) Reverse transcription-polymerase chain reaction and (*b*) Western blot analyses for expression of PDGF-B and PDGFR-β in MSCs and KM12SM cells. PDGFR-beta in MSCs was phosphorylated by coculture with KM12SM cells. Phosphorylation of PDGFR-β in MSCs was inhibited by 1 μM imatinib. (*c*) Migratory ability of MSCs evaluated by transwell assay. The tumor tropism of MSCs was impaired by imatinib treatment, but 1 μM imatinib did not affect proliferation of MSCs (*d*). (*e*) Dose–response curve for imatinib and its growth inhibiting effect in KM12SM cells. *$p < 0.05$, bars: SE.

Migration assay

The migratory ability of MSCs was assayed with the use of a 24-well microchamber plate with uncoated inserts (8 μm pore size, Corning Costar, Tokyo, Japan). Either 2.0×10^4 KM12SM cells in DMEM with 0.5% FBS or medium alone was plated into the lower chambers. After 24 hr of incubation at 37°C, upper chambers containing 2.0×10^4 MSCs in DMEM with 0.5% FBS or 0.5% FBS and 1 μM imatinib, were set into the lower chambers. Three wells were used for each experiment. After 28 hr of incubation at 37°C, inserts were fixed with 10% buffered formalin solution and stained with hematoxylin. The cells on the upper surface of the membranes were removed with cotton swabs. The number of migrating cells was counted in three random fields per filter at 200× magnification.

Proliferation assay

The effect of imatinib on the proliferation of KM12SM cells was analyzed. KM12SM (4.0×10^5) cells were seeded in a 6-well plate in DMEM with 0.5% FBS and 0, 0.5, 2.0, 4.0, or 8.0 μM imatinib. The medium was changed every day, and the number of cells was counted on days 3 and 6 ($n = 6$ in each group).

In vitro growth of KM12SM cells was measured with a Cell Proliferation Biotrak ELISA System, version 2 (Amersham Biosciences, Piscataway, NJ), according to the manufacturer's instructions. Cells were seeded in a 96-well plate at a density of 0.5×10^4 cells/well and incubated overnight in 200 μL culture medium containing 10% FBS. After incubation for 24 hr, cells were cultured in serum-free culture medium containing 10 μM BrdU with or without imatinib for 24 hr, and cell proliferation was measured in a plate reader (Microplate Manager 5.2.1, BIO-RAD, Hercules, CA) at 450 nm.

Western blot analysis

MSCs were cultured in serum-free culture medium for 1 hr and then stimulated with 10 ng/mL PDGF-BB for 10 min. Furthermore, to determine whether PDGFR-β in MSCs is phosphorylated by co-culture with KM12SM cells, 2.0×10^5 MSCs in serum-free culture medium were plated into the lower chambers, and 2.0×10^5 KM12SM cells were cultured in a 6-well microchamber plate with uncoated inserts (0.4